

START-TO-END SIMULATIONS OF NANOMETER-EMITTANCE BEAM TRANSPORT THROUGH AN EMITTANCE EXCHANGE BEAMLINE

B. N. Temizel Ozdemir*, G. Ha, Northern Illinois University, DeKalb, IL, USA

Abstract

We present start-to-end simulation study of the transport of a few pico-Coulomb, nanometer-emittance beam through an emittance exchange (EEX) beamline. EEX with nanometer-emittance beams has potential to enable research opportunities utilizing tunable and high quality attosecond bunches and nanometer-scale longitudinal bunch trains. To account future possibility of experimental demonstrations, the simulation implemented existing EEX beamline at Argonne Wakefield Accelerator (AWA) facility. Simulation was conducted using General Particle Tracer (GPT) and ELEGANT code.

INTRODUCTION

A recent simulation study demonstrated the feasibility of generating sub-micron-scale longitudinal density modulation via an asymmetric emittance exchange (EEX) beamline [1]. In this study, an idealized 6D Gaussian beam was transported through an asymmetric EEX beamline, and the initial transverse modulation with periods of both 1 μm and 3 μm was successfully converted into longitudinal modulations with periods of 800 nm and 230 nm, respectively. While the conversion was successful, the 6D Gaussian beam model ignores various characteristics typically present in photoinjector beams. Here, we explore whether a realistic beam from a photoinjector can still achieve longitudinal modulations comparable to those obtained from a 6D Gaussian beam. Injector simulations were carried out using General Particle Tracer (GPT) [2] and the following asymmetric EEX beamline was simulated using Elegant [3]. Argonne Wakefield Accelerator facility (AWA) and its EEX beamline are modeled.

BEAMLINE LAYOUT

The beamline layout is provided in Fig. 1. The downstream of the linac will be redesigned for experimental demonstrations. The following will be considered in the simulation study to generate nano-scale modulations. A transmission electron microscopy (TEM) grid will be placed after the last accelerating cavity to scatter a portion of the beam and produce transverse density modulations with a period of 12.5 microns. The modulation produced by the TEM grid will then be adjusted in the following demagnification section to produce 3 micron modulations while meeting other beam requirements at the entrance of the asymmetric EEX beamline. Requirements are provided in Ref. [1].

The asymmetric EEX beamline consists of two doglegs with different bending angles and a transverse deflecting cavity (TDC) placed between them. To mitigate aberrations, a

fundamental mode cavity (FMC) and five sextupole magnets are included in the beamline [1]. The EEX beamline is also illustrated in Fig. 1, and relevant parameters are summarized in Ref. [1].

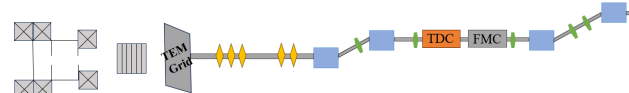


Figure 1: Beamlne Layout.

INJECTOR SIMULATIONS

A multi-variable scan was performed using GPT [2] to identify operational points that satisfy the beam requirements for generating nanometer-scale modulations. As outlined in Ref. [1], the normalized transverse emittance must be on the order of tens of nanometers to preserve nano-scale modulations. We performed various injector scans for a 1 pC charge, as chosen in Ref. [1].

Several important behaviors were observed from the results. To satisfy the emittance requirement, the laser spot diameter must be below 300 μm . The laser pulse length should be in the range of 5-6 ps to produce an rms bunch length of approximately 400 μm , which meets the length requirement. Another notable observation is that the matching solenoid current does not significantly affect the projected transverse emittance. Unlike photoinjectors operating at O(100) pC or higher, the emittance varied by only 5 nm over the scan range as shown in Fig. 2. Therefore, it can be used primarily as a beam size controller.

The laser diameter was set to 180 μm , which corresponds to a normalized emittance of approximately 60 nm. To count the loss from a TEM grid, we raised the charge to 2 pC and scanned bucking-focusing (BF) solenoid current and gun phase. The laser pulse was set to a flat-top profile with a length of 6.4 ps FWHM. Transverse beam size at the TEM grid needs to be set to 400 μm , so the matching solenoid current was set to 175 A.

The new scan results are shown in Fig. 3. The optimal operating point was found at gun phase of 24° and BF solenoid current of 475 A, providing a horizontal rms beam size ($\sigma_{x,i}$) of 413.84 μm , and rms bunch length ($\sigma_{z,i}$) of 403.74 μm , a normalized transverse emittance ($\epsilon_{nx,i}$) of 75.32 nm. The linac phase was set to + 3.6° from the crest to minimize the energy spread.

DENSITY MODULATION AND QUADRUPOLE DEMAGNIFIER

A 2 pC electron beam is used for density modulation generation so that the remaining charge can be a 1 pC. We used

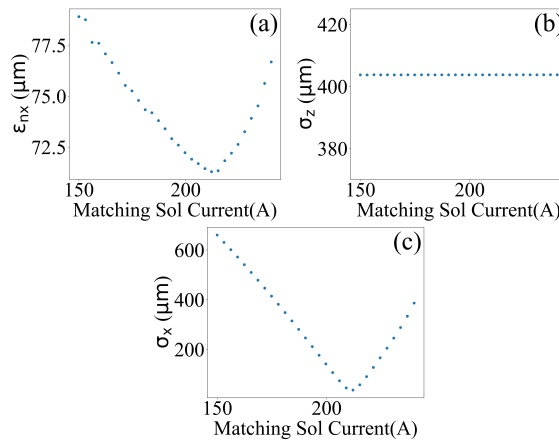


Figure 2: Matching solenoid current scan. Each panel shows the response of (a) normalized horizontal emittance, (b) longitudinal rms beam size, and (c) horizontal rms beam size.

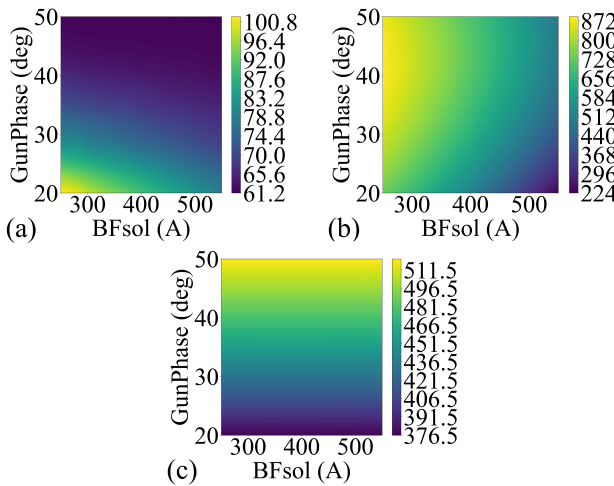


Figure 3: 2D scan over BF solenoid current and gun phase. The colors show the variation of (a) normalized horizontal emittance, (b) horizontal rms beam size, and (c) rms bunch length.

a Python-defined mask to mimic a TEM grid for simplicity. The mask has a periodicity of $12.5 \mu\text{m}$ and a bar thickness of $6.25 \mu\text{m}$, producing a density modulation on the transverse profile as shown in Fig. 4 (a).

A quadrupole demagnifier, shown in Fig. 5(a), was designed to satisfy the following requirements: (i) a demagnification factor of 4.2 to reduce the initial modulation period from $12.5 \mu\text{m}$ to $3 \mu\text{m}$; (ii) transverse rms beam sizes around $100 \mu\text{m}$ to suppress second-order effects; (iii) Minimal transverse divergences; (iv) $R_{12} = 0$ to preserve the transverse modulation.

The quadrupole strengths required to achieve this magnification and satisfy the imaging condition are listed in Table 1. The corresponding beam envelope is given in Fig 5(b). It is worth noting that the footprint of the demagnifier must be less than 2 m due to physical space limitation.

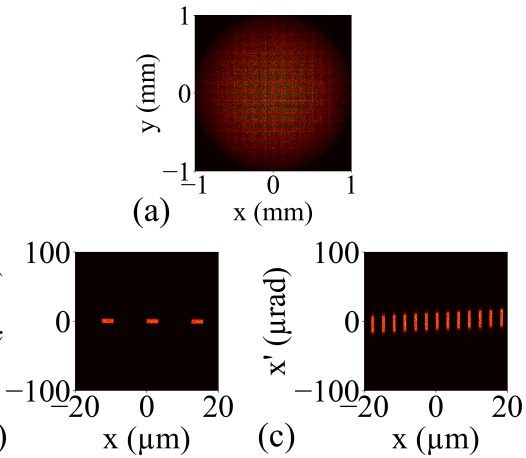


Figure 4: Transverse modulation by TEM grid and demagnifier. (a) Beam image after a mask. The panel (b) and (c) shows transverse phase spaces before and after a quadrupole demagnifier, respectively.

Table 1: Quadrupole strengths for demagnifier. Positive values correspond to horizontal focusing.

Index	Q1	Q2	Q3	Q4
Strength	6.83 m^{-1}	-7.11 m^{-1}	4.54 m^{-1}	6.66 m^{-1}

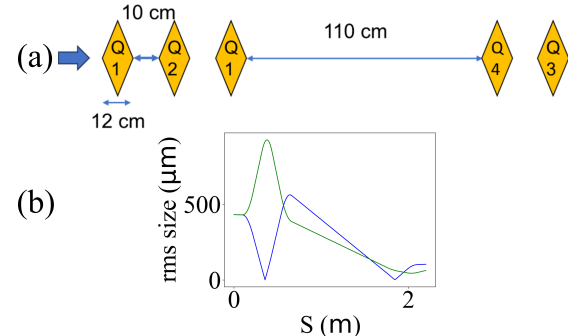


Figure 5: Quadrupole demagnifier. (a) Layout of quadrupole demagnifier. (b) beam envelope inside the demagnifier.

START-TO-END SIMULATION RESULTS

A realistic beam obtained from injector simulations was modulated by the Python-defined mask and adjusted in the demagnifier section. This transport assumed linear transfer. After the demagnification, the beam was tracked through an asymmetric EEX beamline using ELEGANT [3]. To estimate the impact of using a realistic beam, the tracking results were compared with those from a previously studied ideal 6D Gaussian case. Note that the realistic and ideal beams have different initial modulation periods: $3 \mu\text{m}$ for the realistic beam and $1 \mu\text{m}$ for the ideal beam.

Figure 6 presents a comparison of the longitudinal phase spaces at the exit of the EEX beamline. The ideal case shows a clear modulation pattern with a bunching factor of 0.172 at a period of 176 nm. In contrast, the realistic beam exhibits

degraded modulation quality with a bunching factor of only 0.074 at a period of 500 nm. These results indicate the impact of using a realistic beam.

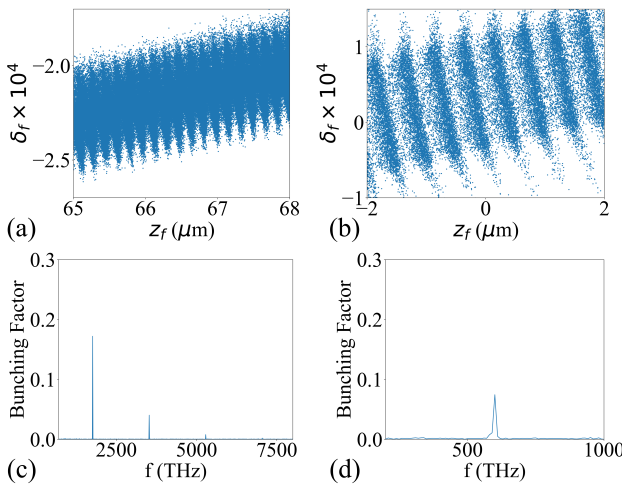


Figure 6: Longitudinal phase spaces downstream of the EEX beamline. (a) and (b) show longitudinal phase spaces at the exit of the beamline for 6D Gaussian and realistic injector beam, respectively. (c) and (d) show corresponding frequency spectra.

SECOND ORDER EFFECTS

To investigate the quality degradation, we analyzed the impact of second-order terms because the two input beam conditions clearly deviated from those of the ideal beam. These are (1) a relatively large vertical phase space slope and (2) a nonlinear longitudinal chirp from RF curvature, as shown in Fig. 7. Problematic second-order terms can be identified using the second-order transport matrix (T), which relates the initial and final coordinates, \mathbf{X}_i and \mathbf{X}_f . This matrix can be calculated from simulated particle distributions as,

$$T = (\mathbf{X}_f \mathbf{X}_i^T)(\mathbf{X}_i \mathbf{X}_i^T)^{-1}, \quad (1)$$

where $\mathbf{X} = (x, x', y, y' z, \delta)^T$. The final longitudinal coordinate can be expressed as,

$$z_f = z_i + R_{56} + \sum_{i,j} T_{5ij} \mathbf{X}_i \mathbf{X}_j. \quad (2)$$

In this study, we do not perform a full second-order characterizations but focus on the terms related to the aforementioned factors.

To identify the dominant contributors to the modulation degradation, we visualized the longitudinal phase space at the exit of the EEX beamline, with colors indicating the particles' initial coordinates: y , y' , and δ . Figure 8 shows a clear dependence of particle spread on these initial coordinates. This indicates strong second-order correlations via $T_{534} yy'$, $T_{544} y'^2$ and $T_{566} \delta^2$. These terms degrade the modulation because they were not considered during the sextupole optimization for the ideal beam case, in which the

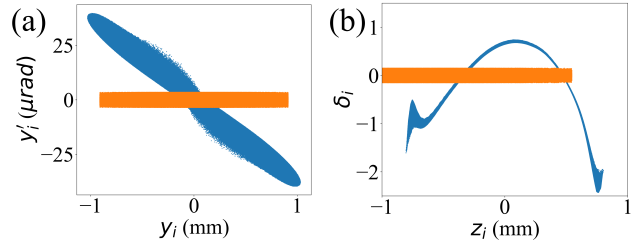


Figure 7: Comparison of the ideal and realistic beams (orange: 6D Gaussian and blue: realistic beam). (a) Initial vertical phase space. (b) Initial longitudinal phase space with δ_i scaled by 10^4 and 10^3 for realistic and 6D Gaussian beams, respectively.

incident transverse slope and chirp were both zero. However, it is also important to note that all of these terms can be mitigated by re-optimizing the sextupole magnets.

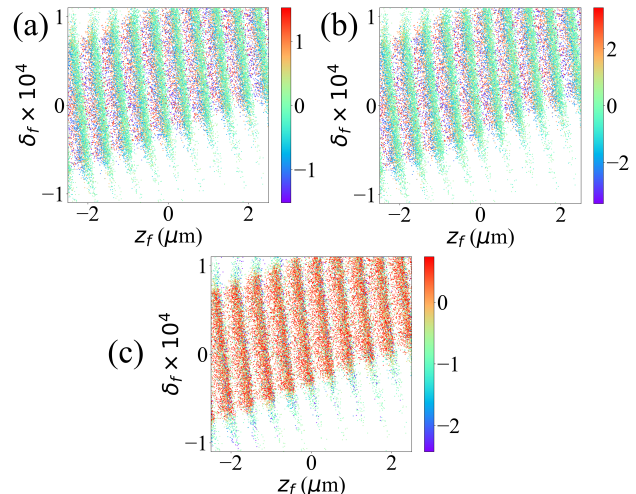


Figure 8: Longitudinal phase space at the exit of asymmetric EEX. For each panel, color represents (a) vertical position (y_i), (b) vertical divergence (y'_i), and (c) energy spread.

SUMMARY

To evaluate the impact of a realistic beam on nano-scale modulation generation, we conducted a comparative study between an ideal 6D Gaussian beam and a beam obtained from AWA injector simulations. The realistic beam, which had unwanted correlations in vertical and longitudinal phase spaces, led to particle spread and a reduction in modulation amplitude. However, it was worth noting that the modulation remains clearly visible at the EEX exit. Furthermore, the degradation sources were identified, and they are factors that can be effectively mitigated by re-optimizing the sextupole magnets. Therefore, the impact of the realistic beam can be under control, and the generation of nano-scale modulation using an asymmetric EEX beamline remains promising.

REFERENCES

- [1] G. Ha *et al.*, “Coherent radiation from initially modulated beams using emittance exchange at the argonne wakefield accelerator”, *Nucl. Instrum. Methods Phys. Res., Sect. A*, vol. 1075, p. 170 387, 2025.
doi:10.1016/j.nima.2025.170387
- [2] M. J. De Loos and S. B. Van der Geer, “General Particle Tracer: A new 3D code for accelerator and beamline design”, in *Proc. EuPAC'96, Sitges, Barcelona, Spain, Jun. 1996*, p. 1241. <https://cds.cern.ch/record/860825>
- [3] M. Borland, “Elegant: A flexible sdds-compliant code for accelerator simulation”, Argonne National Laboratory, Lemont, IL, USA, Tech. Rep. LS-287, 2000. doi:10.2172/761286